Journal of Food Engineering 281 (2020) 110004

Contents lists available at ScienceDirect

Journal of Food Engineering

journal homepage: http://www.elsevier.com/locate/jfoodeng

Dimensional change and cook loss during heating of fish: Problem formulation and semi-empirical modeling approach

Marthe J. Blikra [a,b,*], Åse V. Hodnefjell [b,c], Aberham H. Feyissa [b], Dagbjørn Skipnes [a]

[a] Nofima, Norwegian Institute of Food, Fisheries and Aquaculture Research, Norway
[b] DTU Food Production Engineering, Denmark
[c] Norwegian University of Life Science, NMBU, Ås, Norway

A B S T R A C T

Shrinkage of cod filets and loins during heating is associated with unwanted changes in the product appearance and eating properties, including liquid loss, loss of juiciness and increased hardness. In this paper, shrinkage of minced cod filets exposed to 45–100 °C for up to 1800 s in a convection oven with 100% relative humidity was investigated and related to degree of mass loss. The result was compared to data for cut (non-minced) samples of the same dimension. A kinetic prediction for the mass loss was developed, and it was found that the volume of shrinkage could be approximated by the volume of mass loss. The kinetic prediction was coupled with a model for heat transfer to investigate the effect of shrinkage on the temperature prediction. Further work should include investigation of the effect of the fish macrostructure orientation on shrinkage, as well as optimization of the prediction and validation for large samples such as whole loins.

1. Introduction

During heating of fish muscle (e.g. filets), several changes occur which are biochemical and physical/mechanical in nature. The changes affect both appearance and eating properties of the fish which are important for the consumers, and therefore also for stakeholders in the fish supply chain, especially food manufacturers (industries preparing ready meals). In the case of heat processing of fish filets, shrinkage is one of the changes that lead to quality loss. For cod, shrinkage during heating can be severe, which directly affects the size and weight of the sold ready cooked filet compared to the uncooked filet. This means that there may be substantial losses in raw material during the processing from raw to heated filet, e.g. cook loss. Moreover, and of importance to the consumers, severe shrinkage may have a direct effect on texture and moisture loss, which may reduce juiciness and increase hardness in the product. In some cases, shrinkage also affects the rate of heat transfer, which when unaccounted for may cause differences between predicted and measured temperature profiles during heating. This may render models for heat transfer unsuitable for prediction of temperature-dependent phenomena such as inactivation of bacteria and retention of nutrients, which may be vital for models constructed for process optimization.

To account for shrinkage during heating, the phenomena may be predicted using mathematical modeling. Apart from strictly empirical regression analysis (Mayor and Sereno, 2004), two major strategies to modeling shrinkage during heating or drying of foods has been employed: a) shrinkage based on conservation of mass or volume in relation to expelled moisture (e.g. Feyissa et al., 2009; Dhall and Datta, 2011), and b) shrinkage based on conservation of momentum/pressure accounting for changes in mechanical deformation properties (e.g. Defraeye and Radu, 2018). Both of these approaches can be considered fundamental, and in this paper, the former approach was used. To the best of our knowledge, there are no previous works considering prediction of volumetric shrinkage occurring during heating of fish, and very little research on heat-induced shrinkage of fish in general. The research found predicting heat-induced shrinkage in fish (salmon) looked solely at area shrinkage, and the change in thickness of the samples were not measured (Kong et al., 2007; Ovissipour et al., 2017). Most of the research studying muscle shrinkage during heating use meats, typically beef, as a raw material (e.g. Oroszvári et al., 2005a, 2005b; Oroszvári et al., 2005; Barbera and Tassone, 2006). This research may give some information regarding what can be expected for other types of muscle tissue, such as cod muscle. However, given differences in composition, protein denaturation temperatures, and structure between cod and beef, research specific to cod is also needed both to enable accurate predictions and to facilitate understanding of the mechanisms in play during heat-induced shrinkage.

Shrinkage of muscle foods is a complex issue, and in fish such as cod the degree of complexity is increased compared to for instance beef due to the muscle structure orientation of the fish. Cod muscle is arranged

* Corresponding author. Nofima, Norwegian Institute of Food, Fisheries and Aquaculture Research, Norway.
E-mail address: marthe.blikra@nofima.no (M.J. Blikra).

https://doi.org/10.1016/j.jfoodeng.2020.110004
Received 14 November 2019; Received in revised form 29 January 2020; Accepted 1 March 2020
Available online 2 March 2020

into myotomes, which are thin sheets of muscle connected to the bone and skin, causing contraction and swimming motion in the alive fish (Fig. 1). The myotomes are surrounded by connective tissue and stack horizontally. The added complexity in the shrinkage phenomenon is caused by the spatial orientation of the myotomes, since when cut into a filet, loin or other shape, myotomes are often curved compared to the axes of cutting. The orientation and degree of curviness of the myotomes are observably different from one specimen to the next, and this biological deviation may depend on for instance the size of the whole fish and the position of the muscle piece in the filet. In addition, the width of myotomes differs both within one sheet and between sheets, which adds to the complexity. When preparing samples for studying heat-induced shrinkage in the lab, the differences in the orientation of cut samples may be more important for the measured result than the laboratory set-up, which may result in false-negative correlations.

In an attempt to simplify the complex issue of shrinkage and investigate the effect of temperature and time on the degree of shrinkage in cod, we removed the muscle fibers from their original macrostructure by mincing the filet. In this way, the behavior of the fibers could be investigated without influence of the muscle fiber orientation. The results were compared to data for cut (un-minced) samples of the same dimension. The amount of moisture loss was kinetically analyzed, and we investigated whether the change in weight could adequately describe the shrinkage phenomena during cooking of fish patties.

2. Experimental methods

2.1. Raw material

Two-year-old cod (*Gadus morhua*) from the Aquaculture research station in Tromsø with an average weight of 3.75 kg was used (December 2017). The fish was starved for 9 days, sacrificed by a blow to the head, and bled in seawater at 5.7–6.0 °C for 25 min. The fish was then put on ice until direct filleting and deskinning to filet weights of 373 ± 75.8 g, individual packaging in plastic bags and Styrofoam containers with ice and absorbent, and transportation overnight to our lab. Still at 0 °C, the fish were put in storage at 0–2 °C to undergo *rigor mortis*. After 5 days, the filets were cut into 2–4 pieces according to filet size, quick-frozen directly at −60 °C, vacuum packed at 92.2% to avoid thawing, and stored at −80 °C until analysis (14–16 mo) to maintain freshness and avoid major changes in water state.

2.2. Sample preparation

For kinetic analysis of minced samples, 3–4 cod loins were thawed overnight at 0–2 °C prior to grinding together using a coarse grinder (Robot-Coupe R5A, Bourgogne, France) for 4–5 s. The batch was kept on ice under plastic film throughout the experimental period. Prior to heat treatment, minced cod was shaped into a cylinder of height 9.9 mm and diameter 30 mm using a custom-made steel stencil pipe of the same dimensions. A thin layer of cooking fat was added between the baking tray and the samples to facilitate free contraction of the samples during heating.

For analysis of small pieces of whole fish, cod loins were put at −30 °C overnight, 0–2 °C chill room for 30–60 min, and then cut to a uniform thickness using a meat slicer. A heavy duty round hollow punch – a hand-held device with a sharp-edged pipe attached to a handle – was used to cut the slices into cylinders of approximately equal dimension as minced samples (height: 9.1 ± 0.9 mm; diameter: 28.5 ± 0.6 mm). For analysis of the density of cook loss, the sample underwent the same temperature treatment and slicing as described for cylindrical whole fish samples. The slices were then cut into small cubes of dimensions 3 × 2 cm using a sharp knife and a paper stencil.

2.3. Measurements of cook loss and dimensional change after heating

The samples were heated at 100% relative humidity setting in a Metos System Rational oven (MSCC 61, Kerava, Finland). Prior to analysis, the oven was pre-heated (≥20 min) at temperatures from 45 to 100 °C, with a fan speed setting of 3/5, and the samples were equilibrated for 30 min in room temperature (19 °C) under plastic film. During experiments, the baking tray with the fish samples was placed in position 2 from the bottom (approx. 1/3 up), with direct exposure from the oven fan from one side. All cylindrical samples were heated in a semi-circle arrangement allowing equal fan-exposure of the six parallel measurements. An additional test sample with a centrally positioned thermocouple (SSA-TF, Ellab Validation Solutions, ±0.37 °C) was added to the tray to keep track of the temperature development during heating and cooling. After cooking, samples were transferred to a room tempered stainless steel baking tray and cooled in a chill room at 0–2 °C until the test sample reached 19 °C in the core (4–5 min). The samples were then placed in room temperature under plastic film for 15 min to let them reach temperature equilibrium.

Sample weight was recorded prior to cooking and after temperature equilibration to determine the amount of cook loss (CL), which refers to the liquid exudate dripping from the fish during heating. The volumetric change was then recorded by measurements of height (4 measurements per sample at crossing directions) and diameter (2 perpendicular measurements per sample) using a digital caliper (LiMiT 150 mm, ±0.02 mm).

2.4. Measurements of the density of cook loss

To avoid the uncertainty of exchange of vapor with the oven air, cook loss (CL) was collected after heating cubes of cod sous vide in a water bath. The heat treatments were performed at 40, 50, 60, 70, 80, and 90 °C. A 3 cm glass rod was placed inside the plastic pouch to direct the CL away from the sample. To keep the pouch immersed and the rod vertically positioned beneath the fish, 2 metal nuts were sealed in the bottom of the pouches. After collection of the CL, its apparent density was

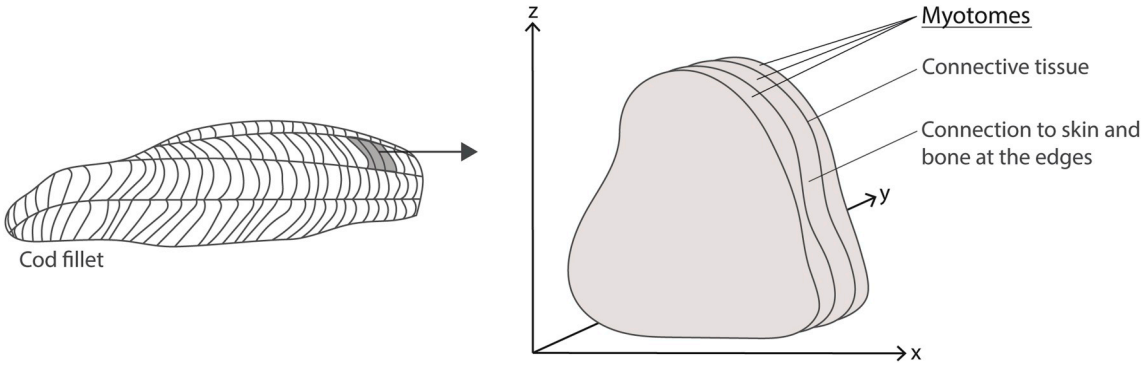

Fig. 1. Muscle structure of cod, emphasizing the interlinkage of myotomes.

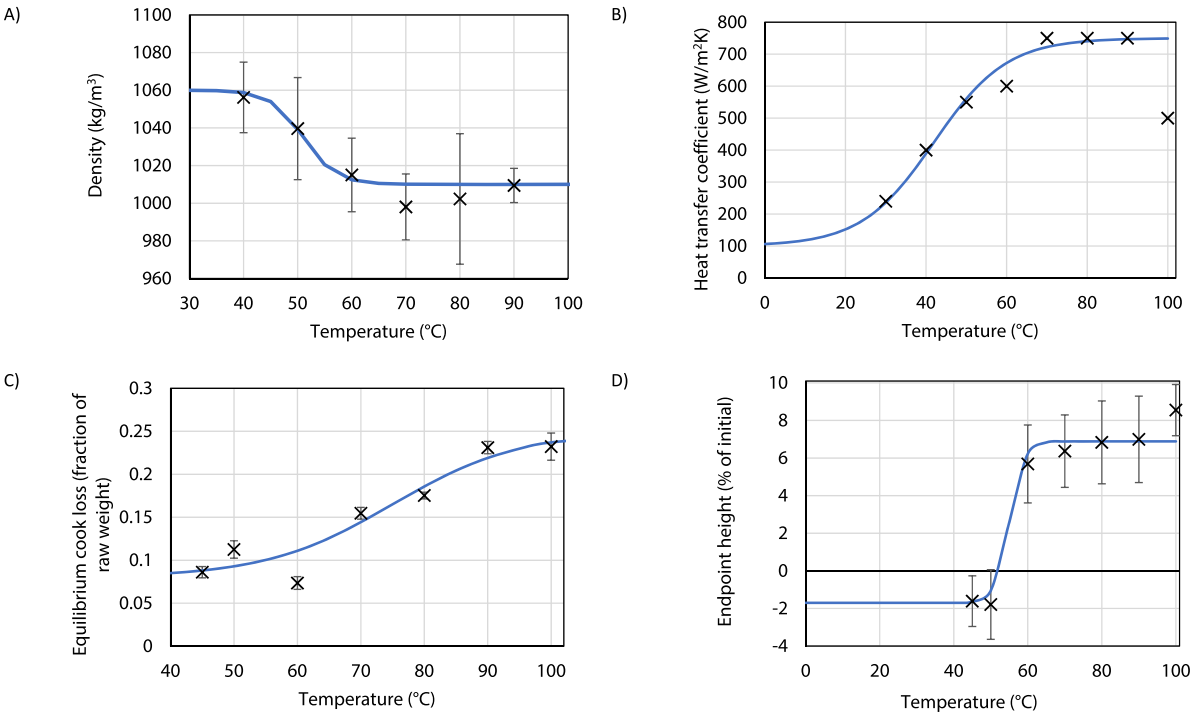

Fig. 2. Sigmoidal relations of measured properties given by Eq. (3) with parameters in Table 1 (lines) plotted together with measured data (±SD, crosses) as a function of temperature. A) Density of the cook loss, accounting for thermal expansion of the water fraction; B) Heat transfer coefficient; C) Equilibrium cook loss; D) Endpoint height (after 1800 s).

measured by reading the volume within a 2 mL graduated pipette, followed by weighing the pipette and subtracting the weight of the pipette without the sample. Prior to measurements, the accuracy of the graduated pipette was tested using water, and an accuracy of ±0.02 g/mL was obtained compared to literature values at the same temperature.

Since all measurements were performed at 20 °C, the thermal expansion of the water fraction of the CL needed to be accounted for separately. The fraction of density change of water compared to the density of water at 20 °C, $y_{\Delta\rho,w}$, was calculated using data from Singh and Heldman (2014) according to Eq. 1

$$y_{\Delta\rho,w} = \rho_{w,T} / \rho_{w,20} \tag{1}$$

where $\rho_{w,T}$ and $\rho_{w,20}$ are the densities at temperatures T (0–100 °C) and 20 °C, respectively. The fraction of density change for the CL was then calculated in terms of the fraction of water in the sample, y_w, according to $y_{\Delta\rho,CL} = y_w(y_{\Delta\rho,w} - 1)$. The fraction of water during sous vide heating of cod was previously found to be 0.9 ± 0.02 between 50 and 90 °C (Nygård, 2019). The density of the CL, ρ_{CL}, accounting for the thermal expansion of the water fraction of the sample, is given by Eq. (2).

$$\rho_{CL} = \rho_{CL,20}(1 + y_{\Delta\rho,CL}) \tag{2}$$

The values were fitted to a sigmoidal function (Eq. (3), Fig. 2) for use in the prediction. In Eq. (3), x_{max} represents the maximum value, which in this case corresponds to the density of CL at 40 °C, 1060 kg/m^3. Since no significant differences were found between 60 and 90 °C, x_{min} is given by the average density at these temperatures, 1010 kg/m^3. The parameters a, b, and c are determined by trial and error and are given in Table 1 together with the other parameters of sigmoidal functions referred to in this work.

$$x = x_{max} + \frac{x_{min} - x_{max}}{1 + a\exp\left(\frac{T[°C] - b}{c}\right)} \tag{3}$$

2.5. Determination of the heat transfer coefficient

The heat transfer coefficient was determined by comparing manual and predicted temperature in an aluminum cylinder (Ø = 30 mm, h = 30 mm). Thermocouples type K (PR Electronics Inc., San Diego, CA; ±0.37 °C) were used for measurement in the geometrical center of the

Table 1
Values for sigmoidal functions (Eq. (3)).

Symbol	Property	x_{max}	x_{min}	a	b	c	Source
ρ_{CL}	Density of CL	1060 kg/m^3	1010 kg/m^3	1	51	3	Measured
h_{air}	Heat transfer coefficient	750 W/m^{2}K	100 W/m^{2}K	1	42	9	Measured
CL_{eq}	Equilibrium CL[a]	0.25 [-]	0.08 [-]	1	75	10	Measured
h_{eq}	Equilibrium height[b]	6.89 [-]	−1.70	1	55	2	Measured
G	Storage modulus	48.2 kPa	14.2 kPa	1	64	5	Blikara et al. (2019, 2020)
WHC	Water holding capacity	0.82 [-]	0.7 [-]	23	25	− 1/0.42	Blikra et al. (2019)

[a] Given as fraction of raw weight.
[b] Given as percent of initial height.

cylinder, and the oven temperature was recorded using a high temperature thermocouple (STC25012E700KT, Ellab Validation Solutions, Hillerød, Denmark; ±0.2 °C; n = 2–3). The oven was pre-heated (≥20 min) using the same settings and an empty baking tray in the same position as described in Section 2.3. The cylinder was hanged centrally in the oven from a cooling rack within 2–3 cm of the baking plate. Since the heating rates were quick and temperatures ≤100 °C, it was assumed that the radiative portion of the heat transfer was neglectable. The heat transfer model of the aluminum cylinder was prepared in COMSOL Multiphysics as will be described in Section 3.4-3.5, substituting the thermophysical properties of the fish with those of the aluminum cylinder (Ghisalberti and Kondjoyan, 1999). The heat transfer coefficients were obtained by adjusting their values in the model until the predicted and measured temperature profiles were in agreement. The obtained values of heat transfer coefficients were then fitted to a sigmoidal function (Eq. (3)) with parameters given in Table 1. The minimum heat transfer coefficient, x_{min}, is the extrapolated minimum heat transfer coefficient which ensures the best fit for the tested oven temperatures (Fig. 2).

2.6. Statistical analysis

Statistical analysis was performed using Minitab® 18.1. One-way ANOVA with 95% confidence interval and Tukey post-hoc test was performed for analysis of significant difference. Kinetic analysis, analysis of linear correlation coefficients (R^2), and calculations of averages and standard deviations were performed using Microsoft Excel 365 ProPlus.

3. Prediction and model formulations

3.1. Process description

In this work, minced fish patties were cooked isothermally in a convection oven at temperatures ranging from 45 to 100 °C, using 100% relative humidity. Heat was transferred from the saturated water vapor in the oven air to the patties by convection, and throughout the patties by conduction and convection. Since the relative humidity of the oven was close to saturation, it was assumed that no net evaporation from the surface occurred, and moisture was only lost form the patties to the surroundings as liquid.

In our experiments, the samples changed both radius and height during heating. The amount and direction of change was dependent on the temperature, as illustrated in Fig. 3. Samples heated at 45–60 °C did not show a consistent behavior between parallels, as some shrunk while others swelled in radius, while samples heated at 70–100 °C always shrunk radially. Regarding change in height, samples heated at 45–50 °C varied from swelling to shrinking, while samples heated at 60–100 °C always swelled. There were significant differences between initial height (9.9 mm) and height after heating for 1800 s for all oven temperatures (P = 0.023 for 45 °C, else P < 0.004). Otherwise, there were no consistent significant differences between heating durations, implying that changes in height were not time dependent. With regards to temperature, there were significant differences between lower heating temperatures (45–50 °C) and higher heating temperatures (60–100 °C) in height after 1800 s.

Given this behavior, the change in radius and height was mathematically predicted in different ways. The change in radius was approached kinetically as will be described in Section 3.3, while a simpler approach was followed for change in height. Given that change in height depended on heating temperature but not time, it was a sigmoidal function of percent average change in height after heating for 1800 s was used for the prediction (Eq. (3), Fig. 2). The maximum value was taken as the average change in height after heating at 60–100 °C, since there were no significant differences between these measurements. The minimum value was taken as the average change in height after heating at 45–50 °C, since no differences were found between these either. It should be noted that the minimum value is negative since the samples shrunk on average when heated at 45–50 °C. The parameters are given in Table 1. The sample height was adjusted prior to the initial time when the complete semi-empirical model was run in COMSOL Multiphysics (see Section 3.5), and all equations employed the adjusted height.

3.2. Expulsion of cook loss

A function of cook loss (CL) in terms of temperature and time was obtained using kinetic predictions performed as described for salmon, shrimp and mussels (Kong et al., 2007; Ovissipour et al., 2013; Ovissipour et al., 2017; Wang et al., 2018). From the general rate law, which describes the change in concentration of a quality attribute, such as CL, in terms of the reaction rate constant, k, the concentration at time t, and time, equations for each reaction order can be attained (e.g. Chang, 2005).

In this work, an apparent equilibrium occurred after longer heating times, and thus equilibrium kinetic equations were employed. The concentration of CL obtained after at the longest heat treatment (1800 s) was termed equilibrium cook loss, CL_{eq}. The 1st order equilibrium reaction is given by Eq. (4), and manipulation of the equation gives the reaction rate constant expressed in Eq. (5) (Kong et al., 2007). The initial concentration of CL is given by CL_i.

$$CL(t) = CL_{eq} + \left(CL_i - CL_{eq}\right)e^{-kt} \tag{4}$$

$$-kt = \ln\left(\frac{CL(t) - CL_{eq}}{CL_i - CL_{eq}}\right) \tag{5}$$

In the case of cook loss, the initial concentration is zero, and Eq. (4) can be simplified to Eq. (6).

$$CL(t) = \left(1 - e^{-kt}\right)CL_{eq} \tag{6}$$

The Arrhenius equation (Eq. (7)) describes the temperature

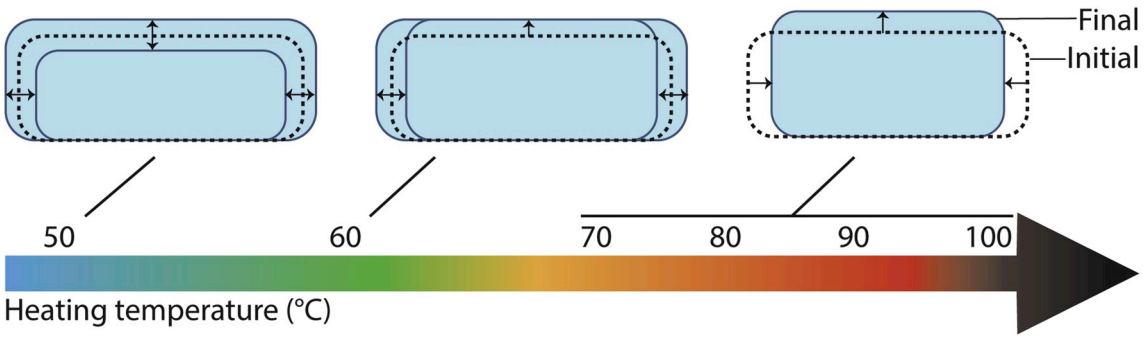

Fig. 3. Shrinkage and swelling behavior of cod patties heated at different temperatures.

Table 2
Input properties in the model and kinetic prediction.

Application	Symbol	Property	Value	Unit	Source
Section 3.2	A	Pre-exponential factor, kinetics of cook loss	0.146	s^{-1}	Measured
	E_a	Activation energy, kinetics of cook loss	12.2	*kJ/mol*	Measured
Section 3.4	$c_{p,cod}$	Specific heat of the cod	3650	J/(kg K)	Skipnes et al. (2007)
	k_{cod}	Thermal conductivity of cod	0.515	W/(m K)	Skipnes et al. (2007)
	ρ_{cod}	Density of cod	1060	kg/m^3	Skipnes et al. (2007)

dependency of the reaction rate in terms of the pre-exponential factor, A_0, and the activation energy, E_a. The activation energy can be found as the slope of the plot $\ln k$ vs. $1/T$, and the pre-exponential factor as the average of $e^{\ln k + E_a/RT}$ for all tested temperatures (Table 2). R is the universal gas constant and T the absolute temperature.

$$k = A_0 e^{-\frac{E}{RT}} \tag{7}$$

3.3. Dimensional change

Previous works have described shrinkage in terms of the mass lost due to evaporation and liquid, which is valid mechanically if the samples are in a wet state (Scherer, 1989; Dhall and Datta, 2011). In this state, the sample retracts at the same rate as mass is lost, and the exterior surface of the sample remains wet (Scherer, 1989). Since our samples were heated at temperatures at or below 100 °C, and the relative humidity used was very high, it is a reasonable assumption that the samples remain in this state throughout the cooking time. In this work, the volume change was therefore predicted semi-empirically using kinetic equations of cook loss.

In the experiments, cylinders of 15 mm radius and 9.9 mm height (Section 2.2) were heated in a convection oven with heat transfer coefficients between 400 and 700 W/m^2K (Section 2.5). Despite the small size of the samples and large heat transfer coefficients, a temperature gradient was established during the first minutes of heating, until the samples reached the same temperature as the oven. The average predicted temperature in the samples reached within 5 °C of the oven temperature after 3.3 min at 100 °C, and shorter times at lower heating temperatures (except 45 °C, with 4.9 min). The reaction rates of cook loss were estimated using the Arrhenius equation (Eq. (7)), and based on this the volume of cook loss could be found as described previously (Section 3.2). When estimating the volume loss of sample due to shrinkage based on the kinetic equations for cook loss (as outlined below), the most correct approach is to use the oven temperature (T_{oven}) in the Arrhenius equation, to mimic the experimental set-up. However, if a mathematical prediction that can be used for any size and shape is to be attained, it is necessary to change the temperature in the equation from that of the oven to the local temperature of the sample (T; Eq. (8)). To check whether applying this change yielded a result within acceptable limits, the complete semi-empirical model (see Section 3.5) was ran first using the oven temperature and then the sample temperature in the Arrhenius equation. As can be seen from Fig. 4, the differences between the resulting radii are negligible, with maximum 0.15% difference (after 46 s). It therefore seems that in this case, the temperature in the samples is sufficiently close to the oven temperature to develop accurate kinetic equations.

$$k = A_0 e^{E_a/RT_{oven}} \approx A_0 e^{E_a/RT} \tag{8}$$

An empirical sigmoidal relation for CL_{eq} was obtained using data for the amount of cook loss expelled after 1800 s (Eq. (3), Table 1). The fraction of CL in terms or raw sample weight ($CL(t)$) was calculated from Eq. (6). The mass of the cook loss was then calculated by multiplication with the initial sample mass (Eq. (9)), and the volume of cook loss ($V_{CL}(t)$) was obtained by dividing by density (Eq. (10); Section 2.4).

$$m_{CL}(t) = CL(t) \times m_i \tag{9}$$

$$V_{CL}(t) = m_{CL}(t)/\rho_{CL} \tag{10}$$

Finally, since the sample was in a wet state (Section 3.1), the volume after time t was given by the volume of cook loss subtracted from the initial volume, $V(t) = V_i - V_{CL}(t)$. Recalling that the change in height (h) was stationary (Section 3.1), the volume change as a function of time was predicted using the change in the radial dimension only. Thus, the radius at time t can be expressed in terms of the volume change (Eq. (11)), and the velocity of the radial change is given by its derivative with respect to time (Eq. (12)). This equation was applied for prediction of the radial shrinkage, as will be described in Section 3.5.

$$r(t) = \sqrt{\frac{\mathrm{V(t)}}{\pi \times h}} \tag{11}$$

$$\frac{d}{dt} r = \frac{d}{dt} \sqrt{\frac{\mathrm{V(t)}}{\pi \times h}} \tag{12}$$

3.4. Heat transfer

The rate of heat transfer is described by Eq. (13), where ρ_{cod}, $c_{p,cod}$, and k_{cod} – the density, specific heat and thermal conductivity – are the material properties of the fish (Table 2). ∇ is the three-dimensional del operator, and T is the temperature (K).

$$\rho_{cod} c_{p,cod} \left(\frac{\partial T}{\partial t}\right) + \nabla \cdot (-k_{cod} \nabla T) = 0 \tag{13}$$

Convective boundary conditions (Eq. (14)) were applied to all external boundaries of the fish sample (Figs. 2–6; e.g. Feyissa et al., 2013):

$$\boldsymbol{n} \cdot (-k_{cod} \nabla T) = h_{air} \ (T_s - T_{oven}) \tag{14}$$

where h_{air} is the convective heat transfer coefficient, measured as described in Section 2.5 and given by Eq. (3) with parameters in Table 1.

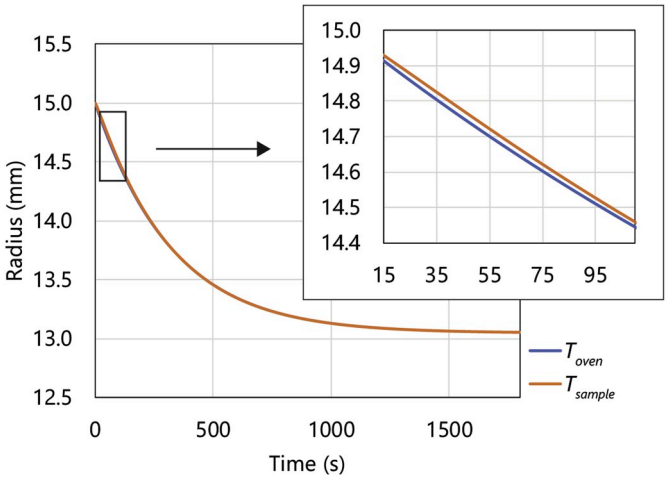

Fig. 4. Comparison of the predicted radius during heating at 100 °C when applying the temperature of the oven versus the local temperature of the sample in the Arrhenius equation (Eq. (8)).

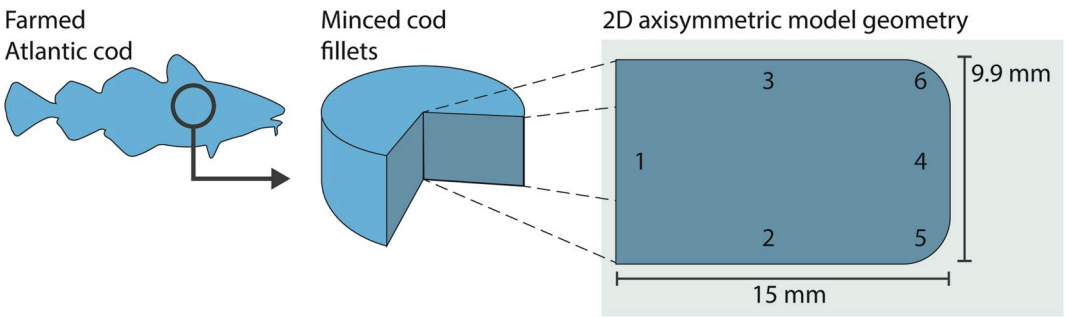

Fig. 5. Raw material processing and model geometry. Numbers 1–6 represent sample boundaries.

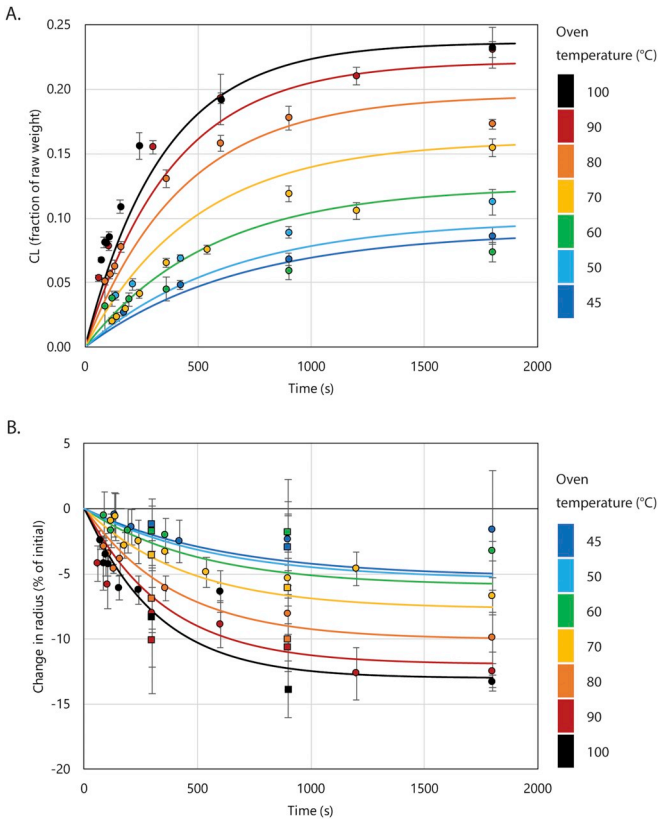

Fig. 6. Measurements of minced cod (±SD, circles), cut cod (±SD, squares), and model predictions (solid lines): A) The amount of cook loss (CL) expelled; and B) The change in radius during heating at 45–100 °C. Identical colors are applied for identical temperatures. (For interpretation of the references to color in this figure legend, the reader is referred to the Web version of this article.)

T_s and T_{oven} are the temperatures at the fish surface and in the oven, respectively.

3.5. Model solution

The complete semi-empirical model, encompassing both the kinetic prediction of dimensional change (Section 3.3) and modeling of heat transfer (Section 3.4), was solved in COMSOL Multiphysics® version 5.4 using the Finite Element Method (FEM). The geometry was a disk constructed as a 2D axisymmetric rectangle with rounded, or filleted, corners (see Fig. 5). The fillets (boundaries 5–6) were added to eliminate sharp edges, which improved the computational convergence. The disk was built with the same radius and height as the minced samples used for measurements of cook loss (Section 2.2). The geometry was meshed using physics-controlled "finer" meshing (maximum element size: 0.88 mm; minimum element size: 0.064 mm; maximum element growth rate: 1.4; curvature factor: 0.4; resolution of narrow regions: 0.7).

For prediction of deformation, the deforming geometry interphase with deforming domain setting was applied. A 2nd order geometry shape was used for the interfase, i.e. 2nd order polynomials were used to represent the geometry shape in the material frame. A Yeoh smoothing type with stiffening factor of 1 was employed. A Lagrange multiplier coupled the mesh displacement (material frame) and the transfer phenomena (spatial frame; ALE method).

The edge of the sample, represented by boundaries 4–6, was prescribed to move in the r-direction at a normal mesh velocity, using the expression in Eq. (12). A prescribed mesh displacement of zero in both directions was applied to boundary 1 in order to avoid dislocation of the full geometry. To keep the position of the top and bottom surface of the sample constant, boundaries 2 and 3 were set to zero normal mesh velocity.

The complete semi-empirical model was run with initial time step of 0.001 s, and a maximum time stepping of 1 s was added to obtain a smooth and accurate prediction throughout the calculation time of 1800 s. The geometry was initially automatically re-meshed when the mesh quality was below 0.5, and subseqently after the quality was below 0.7. Mesh quality is defined as a dimensionless number from 0 to 1, where 1 represents a perfectly regular element, and 0 represents a deformed element. The default measure of Skewness (equiangular skew) was employed. When necessary, backward Euler was used for initialization after remeshing.

4. Results and discussion

4.1. Kinetics of cook loss

When heating fish patties in a convection oven at 100% relative humidity and temperatures ranging from 45 to 100 °C, the amount of expelled cook loss was dependent both on temperature and time. For all heating temperatures, the rate of expulsion was higher in the initial phase of heating, before leveling off and approaching an apparent equilibrium. The behavior was generally also consistent with regards to heating temperature, with more cook loss at higher temperatures. An exception to this generalization was found for samples heated at 60 °C, which yielded less cook loss than samples heated at 45–50 °C.

For heating temperatures 45, 70, 80, 90, and 100 °C, the fraction of cook loss expelled to initial sample weight followed first order reaction kinetics until the equilibrium fraction of cook loss was reached. The same order has also been used to describe the cook loss expelled from salmon, shrimp, and mussels during heating (Kong et al., 2007; Ovissipour et al., 2013, 2017; Wang et al., 2018). The reaction rate constant (k; Eq. (5)) calculated from data for samples heated at 70 °C was very low compared to the tendency expressed by the other heating temperatures and was therefore removed as an outlier during the calculation.

In previous work, Kong et al. (2007) expressed the temperature dependency of the equilibrium level of cook loss of salmon by a linear

function. In our experiments we found that a linear correlation, although of a relatively high correlation value ($R^2 = 0.87$), did not capture the full change of equilibrium cook loss with respect to time. Firstly, the heating temperatures 90 and 100 °C did not show significantly different equilibrium cook loss values, and the linear correlation did not account for this trend. Secondly, the CL equilibrium reached at an oven temperature of 60 °C was lower than that at 45 and 50 °C, when the opposite tendency should be expected from the linear correlation. Instead of using a linear correlation, a sigmoidal type relationship was applied in this work, since this relation yielded an expression closer to the experimental data. The function is illustrated in Fig. 2 and given by Eq. (3) with parameters in Table 1.

The non-linear tendency of the equilibrium CL is not unexpected, since several changes in protein configuration (Blikra et al., 2019, 2020), cell membrane integrity and the resulting permeability (Halder et al., 2011) occur between 40 and 80 °C. It seems that the equilibrium cook loss reflects these changes. In the experiments of Kong et al. (2007), all heating temperatures were above the temperatures of protein denaturation, and this could explain why a linear temperature dependency was found in their experiments.

4.2. Model prediction and validation

The current semi-empirical model is able to predict the dimensional change coupled with the temperature rise of the samples, as exemplified for a sample heated at 100 °C in Fig. 7. A temperature gradient is formed in the initial phase of heating, with lower temperatures found in the geometric core of the sample. After 200 s, the predicted core temperature of the sample approaches the oven temperature. Simultaneous with the temperature development, the sample is shrinking in the radial dimension. The shrinkage continues after the temperature of the sample is uniform, until an equilibrium value is approached at 13.0% shrinkage. When heating at lower temperatures, the amount of predicted shrinkage after 1800 s decreased. At 70–100 °C, 7.6–11.9% shrinkage was predicted, and 5.0–5.8% was predicted between heating temperatures 45–60 °C.

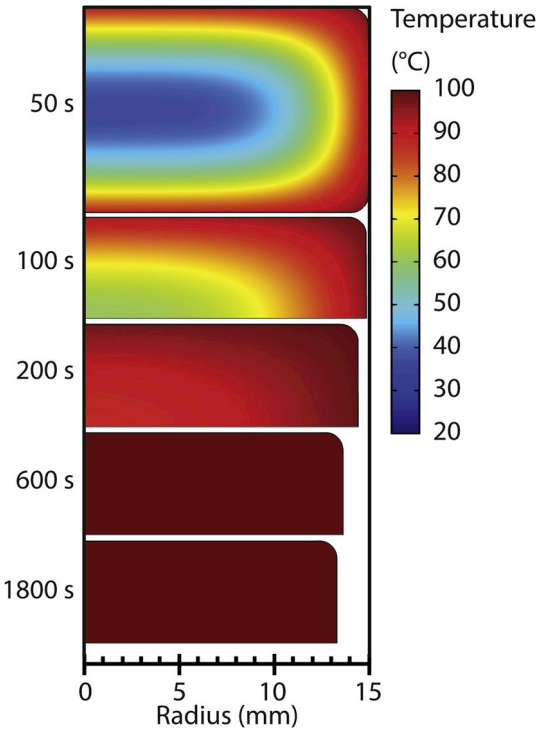

Fig. 7. Predicted temperature profile of the axisymmetric cod patty heated at 100 °C with the corresponding heat-induced dimensional change.

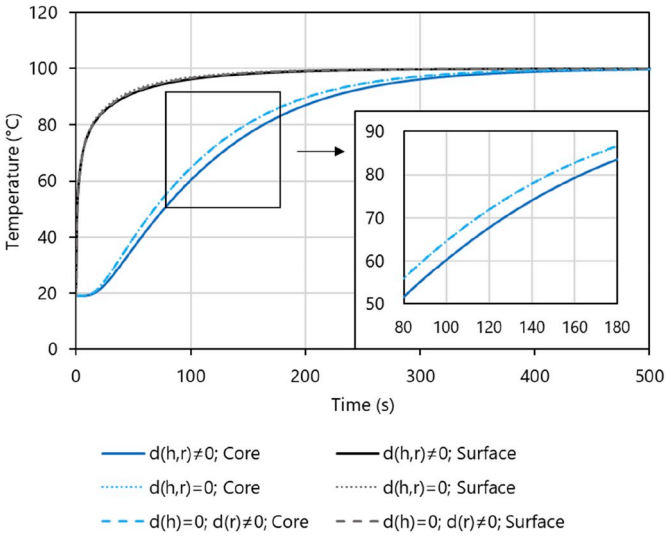

Fig. 8. The effect of dimensional change on the predicted temperature. Model settings: 1) d(h,r)≠0: model ran with change in height and radius; 2) d(h,r) = 0: model ran with no change in any dimension; and 3) d(h) = 0; d(r)≠0: model ran with change in radius but not in height.

Incorporating changing dimensions into a model of heat transfer can sometimes lead to altered temperature predictions. In this work, the predicted core temperature was altered when the change in height was included in the prediction, compared to not including change from the initial height of the samples (Fig. 8). No difference between temperature predictions was found with and without change in radius. This is not unexpected since the heat transfer is more sensitive to changes the smallest dimension of a sample.

Fig. 6b shows the predicted change in radius with the experimental data. In the figure, negative values indicate reduction in radius, i.e. shrinkage, while positive values indicate increase in radius, i.e. swelling. The prediction corresponded well with the measured radius of minced and cut samples between oven temperatures 70–100 °C. This indicates that at these temperatures, empirically measured cook loss can be used to assess the degree of shrinkage through mathematical predictions.

The initial change (<500 s) in the radius of samples heated at 50–60 °C was within the standard deviation of the measurements. For longer heating times the prediction showed clear deviations from the average measurements. The individual measurements at these temperatures ranged from swelling behavior to shrinkage, as is prominent from the SD of the measurements at 1800 s. Due to this unexpected result, all measurements at 50 and 60 °C were repeated, and the experimental data report the average and SD of all data collectively. The prediction was also poor for samples heated at 45 °C. At this temperature, the samples lost weight (Fig. 6a), but the average sample dimensions were the same as the initial dimension after heating at 1800 s. These results indicate that shrinkage is not the only mechanism that leads to cook loss.

From the previous sections, we see that volumetric change in cook loss mimics the volumetric change in sample dimension for temperatures above those of protein denaturation. When heating at lower temperatures the relationship between cook loss and shrinkage was not as clear. Heating at 45 °C yielded 8.6 ± 0.7% cook loss after heating for 1800 s, however there were no significant differences in height nor radius between initial dimensions and dimensions after heating for 1800 s, implying that the samples lost mass while maintaining size. For samples heated at 50 °C, 11/60 measurements showed swelling both in radius and height while losing mass, and the same was true for 6/72 samples heated at 60 °C. Rather than reflect measurement uncertainty, these results could point to the mechanisms relating cook loss and shrinkage and their relation to biochemical changes, such as protein denaturation and disruption of cell membranes. These points should be

followed up in later studies of heat-induced dimensional change.

5. Conclusion

In this work, the kinetics of cook loss from cod patties was characterized and used to semi-empirically model coupled shrinkage and heat transfer during heating of cod patties. The amount of cook loss (CL) expelled during heating follow 1st order equilibrium kinetic equations. During cooking of cod patties, the shrinkage occurred mostly in the radial dimension, while the height of the samples marginally increased when heated above 60 °C. It was possible to predict volumetric shrinkage by employing the kinetic equations for expulsion of CL, and the prediction showed good agreement with experimental data of change in radius from 70 to 100 °C heating temperatures. At heating temperatures from 45 to 60 °C, the amount of CL exceeded the dimensional change, and a linear relationship between CL and shrinkage was not obtained.

Cook loss was kinetically predicted using the local temperature in the sample instead of oven temperature, and thus the semi-empirical model is able to predict shrinkage both during fast and slow heating processes. However, such applications should also be validated, especially since the extent and orientation (x, y, z) of shrinkage of cod may depend on shape and size.

The insight from this work can contribute to building sophisticated predictive models which can be used to optimize and tailor food products containing cod. Such models can be valuable tools for use in the industry, institutional kitchens, and restaurants.

CRediT authorship contribution statement

Marthe J. Blikra: Conceptualization, Methodology, Supervision, Software, Validation, Formal analysis, Writing - original draft, Visualization, Writing - review & editing. **Åse V. Hodnefjell:** Methodology, Validation, Investigation, Writing - review & editing. **Aberham H. Feyissa:** Conceptualization, Writing - review & editing, Supervision. **Dagbjørn Skipnes:** Conceptualization, Writing - review & editing, Supervision, Project administration, Funding acquisition.

Acknowledgements

This work was supported by the Norconserv Foundation, the Research Council of Norway, and the Technical University of Denmark (DTU). We would also like to thank Tale Nygård for her careful measurements of the density of cook loss during her master thesis work at the University of Stavanger, under the supervision of Nofima.

References

Barbera, S., Tassone, S., 2006. Meat cooking shrinkage: measurement of a new meat quality parameter. Meat Sci. 73 (3), 467–474.
Blikra, M.J., Skipnes, D., Feyissa, A.H., 2019. Model for heat and mass transport during cooking of cod loin in a convection oven. Food Contr. 102, 29–37.
Blikra, M.J., Jessen, F., Feyissa, A.H., Vaka, M.R., Skipnes, D., 2020. Low-concentration salting of cod loins: the effect on biochemical properties and predicted water retention during heating. LWT - Food Sci. Technol. (Lebensmittel-Wissenschaft -Technol.) 118, 108702.
Chang, R., Murdzek, J., 2005. 9. Chemical Kinetics. *Physical Chemistry for the Biosciences*. University Science Books, Sausalito, California.
Defraeye, T., Radu, A., 2018. Insights in convective drying of fruit by coupled modeling of fruit drying, deformation, quality evolution and convective exchange with the airflow. Appl. Therm. Eng. 129, 1026–1038.
Dhall, A., Datta, A.K., 2011. Transport in deformable food materials: a poromechanics approach. Chem. Eng. Sci. 66 (24), 6482–6497.
Feyissa, A.H., Adler-Nissen, J., Gernaey, K.V., 2009. Model of Heat and Mass Transfer with Moving Boundary during Roasting of Meat in Convection-Oven. COMSOL Conference, Milan.
Feyissa, A.H., Gernaey, K.V., Adler-Nissen, J., 2013. 3D modelling of coupled mass and heat transfer of a convection-oven roasting process. Meat Sci. 93 (4), 810–820.
Ghisalberti, L., Kondjoyan, A., 1999. Convective heat transfer coefficients between air flow and a short cylinder. Effect of air velocity and turbulence. Effect of body shape, dimensions and position in the flow. J. Food Eng. 42 (1), 33–44.
Halder, A., Datta, A.K., Spanswick, R.M., 2011. Water transport in cellular tissues during thermal processing. AIChE J. 57 (9), 2574–2588.
Kong, F.B., Tang, J., Rasco, B., Crapo, C., 2007. Kinetics of salmon quality changes during thermal processing. J. Food Eng. 83 (4), 510–520.
Mayor, L., Sereno, A., 2004. Modelling shrinkage during convective drying of food materials: a review. J. Food Eng. 61 (3), 373–386.
Nygård, T., 2019. Liquid Losses from Atlantic Cod (*Gadus morhua*) during Heat Treatment. University of Stavanger: Master thesis.
Oroszvári, B.K., Bayod, E., Sjöholm, I., Tornberg, E., 2005a. The mechanisms controlling heat and mass transfer on frying of beefburgers. Part 2: the influence of the pan temperature and patty diameter. J. Food Eng. 71 (1), 18–27.
Oroszvári, B.K., Sjöholm, I., Tornberg, E., 2005b. The mechanisms controlling heat and mass transfer on frying of beefburgers. I. The influence of the composition and comminution of meat raw material. J. Food Eng. 67 (4), 499–506.
Ovissipour, M., Rasco, B., Tang, J., Sablani, S.S., 2013. Kinetics of quality changes in whole blue mussel (*Mytilus edulis*) during pasteurization. Food Res. Int. 53 (1), 141–148.
Ovissipour, M., Rasco, B., Tang, J., Sablani, S., 2017. Kinetics of protein degradation and physical changes in thermally processed Atlantic salmon (*Salmo salar*). Food Bioprocess Technol. 10 (10), 1865–1882.
Scherer, G.W., 1989. Drying gels: VIII. Revision and review. J. Non-Cryst. Solids 109 (2–3), 171–182.
Singh, R.P., Heldman, D.R., Taylor, S.L., 2014. Appendix A.4 Physical Properties of Water and Air. *Introduction to Food Engineering*. Elsevier, Academic Press, London, England.
Skipnes, D., Østby, M.L., Hendrickx, M.E., 2007. A method for characterising cook loss and water holding capacity in heat treated cod (Gadus morhua) muscle. J. Food Eng. 80 (4), 1078–1085.
Wang, J., Tang, J., Rasco, B., Sablani, S.S., Ovissipour, M., Qu, Z., 2018. Kinetics of quality changes of shrimp (Litopenaeus setiferus) during pasteurization. Food Bioprocess Technol. 11 (5), 1027–1038.